

# Maximally entangled mixed states: Creation and concentration

Nicholas A. Peters, Joseph B. Altepeter, David Branning\*, Evan R. Jeffrey, Tzu-Chieh Wei, and Paul G. Kwiat  
Physics Department, University of Illinois, 1110 West Green Street, Urbana, IL 61801  
(Dated: July 31, 2003)

Using correlated photons from parametric downconversion, we extend the boundaries of experimentally accessible two-qubit Hilbert space. Specifically, we have created and characterized maximally entangled mixed states (MEMS) that lie above the Werner boundary in the linear entropy-tangle plane. In addition, we demonstrate that such states can be efficiently concentrated, simultaneously increasing both the purity and the degree of entanglement. We investigate a previously unsuspected sensitivity imbalance in common state measures, i.e., the tangle, linear entropy, and fidelity.

PACS numbers: 42.50.Dv, 42.65.Lm, 03.67.Mn

By exploiting quantum mechanics it is possible to implement provably secure cryptography [1], teleportation [2], and super-dense coding [3]. These protocols and most others in quantum information processing require a known initial quantum state, and typically have optimal results for pure, maximally entangled initial states. However, decoherence and dissipation may cause the states to become mixed and/or less entangled. As the success of a protocol such as quantum teleportation often hinges on both the purity and the entanglement of the initial state [4], it is important to study the interplay of these properties. Using a source of 2-qubit polarization states [5], we investigate the creation of maximally entangled mixed states, and their concentration [6, 7, 8, 9].

Entangled states have been demonstrated in a variety of systems [10, 11, 12, 13, 14, 15]. In fact, there are several classes of entangled states; maximally entangled and nonmaximally entangled pure states [5, 11, 16], nonmaximally entangled mixed states [17], and the special case of Werner states [18] (incoherent combinations of a completely mixed state and a maximally entangled pure state) have all been experimentally realized using optical qubits. For some time it was believed that Werner states possess the most entanglement for a given level of mixedness. However, Munro et al. [19] discovered a class of states that are more entangled than Werner states of the same purity. These maximally entangled mixed states (MEMS) possess the *maximal* amount of entanglement (tangle or entanglement of formation) for a given degree of mixedness (linear entropy) [20, 21].

By generating states close to the MEMS boundary, we have experimentally explored the region above the Werner state line on the linear entropy-tangle plane [22]. We have also implemented a partial-polarizer filtration/concentration technique which simultaneously increases both purity and entanglement, at the cost of decreasing the ensemble size of initial photon pairs. Though the implementation requires initial state knowledge, we show that MEMS exist for which this “Procrustean” filtering technique [6, 8, 23] is much more efficient than other recent entanglement concentration schemes [24,

25], even after modification to work on MEMS.

The exact form of the MEMS density matrix depends on the measures used to quantify the entanglement and mixedness [21]; here we use the tangle ( $T(\rho) = [\max\{0, \lambda_1 - \lambda_2 - \lambda_3 - \lambda_4\}]^2$ ) [26], i.e., the concurrence squared; and the linear entropy ( $S_L(\rho) = \frac{4}{3}[1 - \text{Tr}(\rho^2)]$ ) [4]. Here  $\lambda_i$  are the square roots of the eigenvalues of  $\rho(\sigma_2 \otimes \sigma_2)\rho^*(\sigma_2 \otimes \sigma_2)$ , in non-increasing order by magnitude, with  $\sigma_2 = \begin{pmatrix} 0 & -i \\ i & 0 \end{pmatrix}$ . For this parameterization, where  $r$  is the concurrence, the MEMS density matrices exist in two subclasses [19],  $\rho_{MEMS I}$  and  $\rho_{MEMS II}$ , which have two and three eigenvalues, respectively:

$$\rho_{MEMS I} = \begin{pmatrix} \frac{r}{2} & 0 & 0 & \frac{r}{2} \\ 0 & 1-r & 0 & 0 \\ 0 & 0 & 0 & 0 \\ \frac{r}{2} & 0 & 0 & \frac{r}{2} \end{pmatrix}, \quad \frac{2}{3} \leq r \leq 1, \quad (1)$$

$$\rho_{MEMS II} = \begin{pmatrix} \frac{1}{3} & 0 & 0 & \frac{r}{2} \\ 0 & \frac{1}{3} & 0 & 0 \\ 0 & 0 & 0 & 0 \\ \frac{r}{2} & 0 & 0 & \frac{1}{3} \end{pmatrix}, \quad 0 \leq r \leq \frac{2}{3}. \quad (2)$$

Our creation of MEMS involves three steps: creating an initial state of arbitrary entanglement, applying local unitary transformations, and inducing decoherence. First, frequency degenerate 702-nm photons are created by pumping thin nonlinear  $\beta$ -Barium Borate (BBO) crystals with a 351-nm Ar-ion laser. Polarization entanglement is realized by pumping two such crystals oriented such that their optic axes are in perpendicular planes. With a pump polarized at  $\theta_1$ , a variable entanglement superposition state  $\cos\theta_1|HH\rangle + \sin\theta_1|VV\rangle$  is created, where  $|HH\rangle$  represents two horizontally polarized and  $|VV\rangle$  two vertically polarized photons [5, 16]. The pump polarization is controlled by a half-wave plate (HWP<sub>1</sub> in Fig. 1) set to  $\theta_1/2$ .

To create the MEMS I, we start by setting the ini-

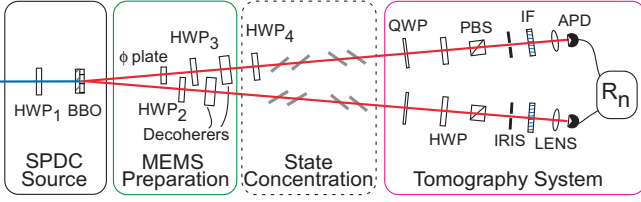


FIG. 1: Experimental arrangement to create, and concentrate MEMS. A half-waveplate ( $HWP_1$ ) sets the initial entanglement of the pure state. The  $\phi$ -plate sets the relative phase between  $|HH\rangle$  and  $|VV\rangle$  in the initial state.  $HWP_2$  and  $HWP_3$  rotate the state into the active bases of the decoherers to adjust the amount of entropy. The tomography system uses a quarter-waveplate (QWP), HWP, and a polarizer in each arm to analyze in arbitrary polarization bases; the transmitted photons are counted in coincidence via avalanche photodiodes. The dashed box contains  $HWP_4$  (oriented to rotate  $|H\rangle \leftrightarrow |V\rangle$  in the first arm of the experiment) and concentrating elements (a variable number of glass pieces oriented at Brewster's angle to completely transmit  $|H\rangle$ , but only partially transmit  $|V\rangle$ ).

tial degree of entanglement to that of the target MEMS. Next a maximum likelihood tomography [16, 27] of this initial entangled state is taken and used to numerically determine the appropriate settings of  $HWP_2$  and  $HWP_3$  in Fig. 1. These waveplates set the diagonal elements of the density matrix to the target values for the desired MEMS. The initial tomography must be precise, because the waveplate settings are critically dependent on the initial state, as well as on the precise birefringent retardation of the waveplates themselves. After the waveplates, the state passes through decoherers, which lower specific off-diagonal elements in the density matrix, yielding the final state. In our scheme, each decoherer is a thick birefringent element ( $\sim 1$  cm quartz, with optic axis horizontal) chosen to have a polarization-dependent optical path length difference ( $\sim 140\lambda$  [28]) greater than the down-converted photons' coherence length ( $L_c \equiv \lambda^2/\Delta\lambda \cong 70\lambda$ , determined by a 10-nm FWHM interference filter placed before each detector), but much less than the coherence length of the pump [29].

The decoherer in each arm couples the polarization with the relative arrival times of the photons [30]. While two horizontal ( $|HH\rangle$ ) or two vertical ( $|VV\rangle$ ) photons will be detected at the same time, the state  $|HV\rangle$  will in principle be detected first in arm one and then in arm two, and vice versa for the state  $|VH\rangle$  (assuming the decoherer slows vertically polarized photons relative to horizontally polarized ones). Tracing over timing information during state analysis then erases coherence between any distinguishable terms of the state (i.e., only the coherence term between  $|HH\rangle$  and  $|VV\rangle$  remains). A sample tomography of a MEMS I is shown in Fig. 2(a).

MEMS II are created by first producing the MEMS I at the MEMS I/II boundary, i.e., the state with  $r = \frac{2}{3}$ . In order to travel along the MEMS II curve, the optical path length difference in *one* arm must be varied from  $140\lambda$ . This couples different relative timings to the  $|HH\rangle$

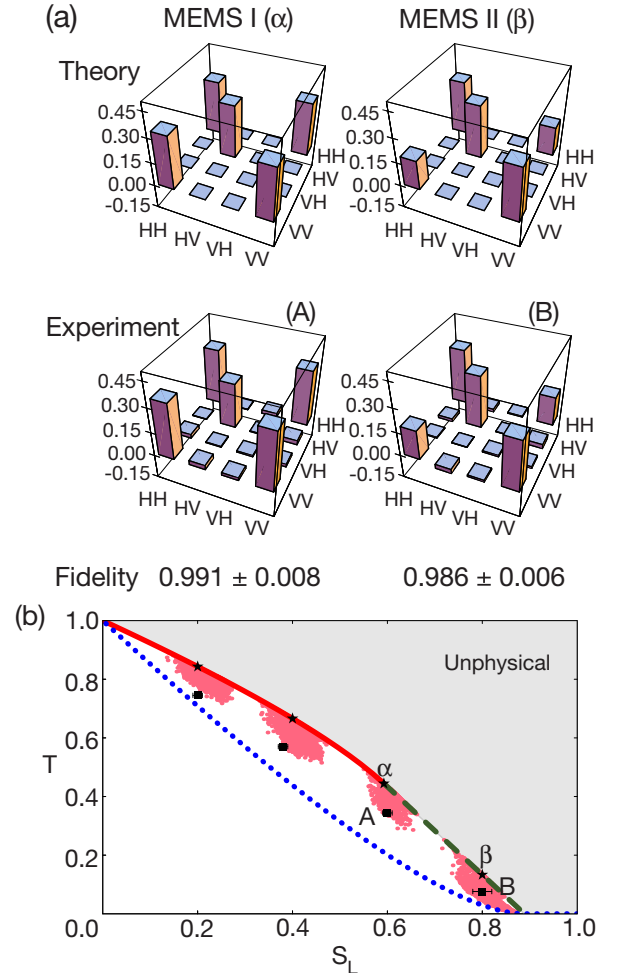


FIG. 2: MEMS data. (a) Density matrix plots of the real components of a MEMS I ( $r = \frac{2}{3}$ ) and a MEMS II ( $r = 0.3651$ ). The imaginary components are negligible (on average less than 0.02) and not shown. (b) Linear entropy-tangle plane. Shown are theoretical curves for MEMS I (solid line), MEMS II (dashed line), and Werner states (dotted line). Four target MEMS are indicated by stars; experimental realizations are shown as squares with error bars. The shaded patches around each target state show the tangle ( $T$ ) and linear entropy ( $S_L$ ) for 5000 numerically generated density matrices that have at least 0.99 fidelity [31] with the target state.  $T=0$  (1) corresponds to a product (maximally entangled) state.  $S_L=0$  (1) corresponds to a pure (completely mixed) state.

and  $|VV\rangle$  states, reducing the coherence between them. For instance, to make the MEMS II (B) in Fig. 2(a),  $140\lambda$  decoherence was used in one arm,  $90\lambda$  in the other. Fig. 2(a) indicates very good agreement between theory and experiment with fidelities of  $\sim 99\%$  (the fidelity [31] between the target state  $\rho_t$  and the measured state  $\rho_m$  is given by  $F(\rho_t, \rho_m) \equiv |\text{Tr}(\sqrt{\sqrt{\rho_t}\rho_m\sqrt{\rho_t}})|^2$ ).

The states (A) and (B) are shown in the  $S_L$ - $T$  plane in Fig. 2(b), along with other MEMS we created. The states do not hit their  $S_L$ - $T$  targets (shown as stars in the figure) within errors, even though the states have very high fidelities ( $\gtrsim 99\%$ ) with their respective targets. To explore the discrepancy, for each target we nu-

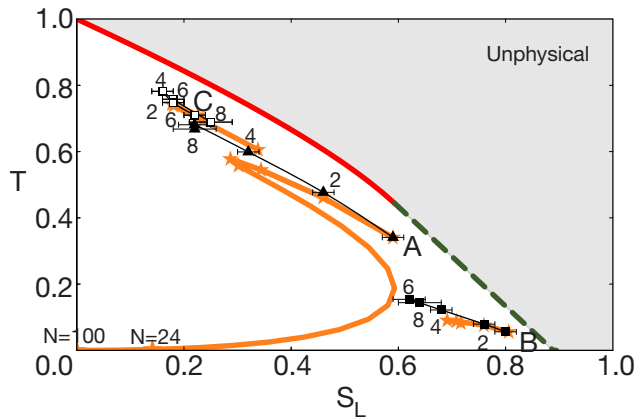


FIG. 3: Concentration data. Shown are concentrations for three initial states, A (triangles) and B (filled squares) as in Fig. 2, and C (open squares), along with the number of partial polarizing glass pieces in each arm. The expected concentrated state path, calculated using [8], is shown with stars. The concentrated states agree with theory for small numbers of glass pieces, but as more slips are used, the state concentrates better than expected. We believe this is due to the extreme sensitivity of the trajectory to small changes in the initial state. However, even in theory, excessive filtration will eventually produce a pure product state (shown as an extension of A’s theory curve), due to small errors in the initial MEMS.

merically generated 5000 density matrices that had at least 0.99 fidelity with the target density matrix. The  $S_L$  and  $T$  of the numerically generated states are plotted in Fig. 2(b) as shaded regions surrounding the targets. The fact that these regions are rather large (and overlap with our measured MEMS) explains our results, but is surprising nonetheless. The unexpectedly large size of these patches arises from the great difference in sensitivity between the state measures of fidelity, tangle and entropy: for small perturbations ( $\delta r$ ) of the MEMS parameter  $r$ , the fidelity is only quadratic in  $\delta r$ , while  $S_L$  and  $T$  are linear in  $\delta r$  [32].

While our initial goal was to produce states of maximal tangle for a given linear entropy, maximally entangled pure states are generally more useful for quantum information protocols. However, in some cases, weakly entangled mixed states may be the only available resource. It is therefore important to study ways to simultaneously decrease the entropy and increase the entanglement of an ensemble of photon pairs (necessarily at the cost of reducing the size of the ensemble). Recently several such entanglement concentration experiments have been reported, relying on two-photon interference effects [24, 25]. An interesting characteristic of MEMS is that they can be readily concentrated by a “Procrustean” method of local filtering [6, 23]. To concentrate we first modify the MEMS using HWP<sub>4</sub> at 45° to exchange  $|H\rangle \leftrightarrow |V\rangle$  in the first arm, changing the non-zero diagonal elements of the MEMS density matrix to  $|HV\rangle\langle HV|$ ,  $|VH\rangle\langle VH|$ , and  $|VV\rangle\langle VV|$ . By reducing the  $|VV\rangle\langle VV|$  element of the rotated MEMS, the outcome

will be driven toward the maximally entangled pure state  $|\phi^+\rangle \equiv (|HV\rangle + |VH\rangle)/\sqrt{2}$ . We achieve this by inserting glass pieces (each piece consisting of four  $\sim 1$ mm thick microscope slides sandwiched together with index matching fluid) oriented at Brewster’s angle, as indicated in the dotted box in Fig. 1. Equal numbers of pieces are used in both arms; they are oriented to nearly perfectly transmit horizontally polarized photons (transmission probability  $T_H = 0.990 \pm 0.006$ ) while partially reflecting vertically polarized photons ( $T_V = 0.740 \pm 0.002$ ).

We concentrated a variety of MEMS. Fig. 3 shows the results for the MEMS I and II of Fig. 2 and an additional MEMS I (C). As the number of glass pieces is increased, the states initially become more like a pure maximally entangled state. For example, in the case of (A), the fidelity of the initial MEMS with the state  $|\phi^+\rangle$  is 0.672. When the state is concentrated with eight glass slips per arm, the fidelity with  $|\phi^+\rangle$  is 0.902; 4.5% of the initial photon pairs survive this filtering process. The theoretical maximum survival probability is 6.4%. Note a characteristic difference between the two MEMS subclasses: MEMS II cannot be filtered into a Bell state.

We now compare the theoretical efficiency of our local filtering scheme with the interference-based concentration proposal of Bennett et al. [7], assuming identical initial MEMS and the same number of photon pairs. We shall compare the average final entanglement of formation ( $E_F$ ) [26] (i.e., the  $E_F$  of the concentrated state multiplied by the probability of success) *per initial pair*. The Bennett et al. [7] scheme was recently approximated by Pan et al. [24], with CNOT operations replaced by polarizing beam splitters; however, due to incomplete Bell state analysis, the probability of successful concentration is only 50% of the original proposal (the recent scheme of Yamamoto et al. [25] is unable to distill MEMS). The first step of both schemes is to perform a “twirling” operation [33] to transform a general entangled state into a Werner state. However, this initial operation usually *decreases* the entanglement, and the scheme with twirling is efficient only when  $r$  is close to 1.

In fact, MEMS I could also be distilled *without* the twirling operation, using the scheme of Pan et al. But then the probability of success depends on the parameter  $r$ . For most MEMS, the maximum distillation efficiency from filtration can exceed that achievable using the interference-based methods [34]. For example, as shown in Table I, when the initial state is a MEMS with  $r = 0.778$ , the two-piece filtering technique has a theoretical  $E_F$  per pair nearly three times higher than the interference scheme without twirling, even though a successful concentration produces nearly the same  $E_F$ . In theory, using 2 to 5 slips achieves both higher entanglement of the successful state and better average entanglement yield. In practice, the filtration technique is *much* more efficient (see the final columns of Table I) [34].

We have demonstrated a tunable source of high fidelity

Concent. method	Prob. of success	$E_F$ when successful	Ideal $E_F$ per pair	Exp. $E_F$ per pair
Twirling [7]	74.8%	0.51	0.19	NA
No Twirling [24]	35.2%	0.80	0.14	$\lesssim 10^{-5}$
Procrustean				
2 pieces	50.4%	0.81	0.41	0.14
4 pieces	26.4%	0.88	0.23	0.07
6 pieces	14.2%	0.93	0.13	0.03

TABLE I: Efficiency comparison of concentration technique of Bennett et al. using ideal CNOT [7], interference-based concentration [24] without twirling, and Procrustean filtering, for an initial MEMS with  $r = 0.778$  and  $E_F = 0.69$ . The scheme of Bennett et al. requires a twirling operation that decreases the initial  $E_F$  to 0.418 before the concentration [33]. In all schemes, except for the final column, we assume the ideal case, i.e., no loss and perfect detector efficiency. To calculate the no-loss result for our filtering scheme, we normalize the measured partial polarizer transmission coefficients (of a single glass piece) to  $T_H = 0.740/0.990$  and  $T_V = 1$ . In the interference schemes, columns 2-4 assume the existence of the required two identical pairs, but in practice this requirement is difficult to achieve [34]. This limitation is reflected in column 5, which lists the average  $E_F$  per initial pair achieved in our experiment, to be compared with the much lower value achievable with current interference method technology.

MEMS. As a consequence of comparing the  $T$ - $S_L$  and fidelity values of generated MEMS with the theoretical targets, we identify and explain an unsuspected difference in sensitivity in these state measures. Furthermore, we have applied a Procrustean filtering technique to several MEMS, realizing a measured efficiency that is well above that achievable using other methods. However, in the limit of very strong filtering, small perturbations in the initial state will eventually dominate the process, yielding only product states (see Fig. 3). In practice, therefore, it may be optimal to combine both methods.

This work was supported by the DCI Postdoctoral Fellowship Program, ARDA and NSF grant # EIA-0121568.

[\*] Present address: *Dept. of Physics and Optical Eng., Rose-Hulman Inst. of Tech., Terre Haute, Indiana, 47803.*

- [1] N. Gisin, G. Ribordy, W. Tittel, and H. Zbinden, *Rev. Mod. Phys.* **74**, 145 (2002); *Focus on Quantum Cryptography*, *New J. Phys.* **4**, 41 (2002).
- [2] C. H. Bennett *et al.*, *Phys. Rev. Lett.* **70**, 1895 (1993).
- [3] C. H. Bennett and S. J. Wiesner, *Phys. Rev. Lett.* **69**, 2881 (1992).
- [4] S. Bose and V. Vedral, *Phys. Rev. A* **61**, R040101 (2000).
- [5] P. G. Kwiat *et al.*, *Phys. Rev. A* **60**, R773 (1999).
- [6] C. H. Bennett, H. J. Bernstein, S. Popescu, and B. Schumacher, *Phys. Rev. A* **53**, 2046 (1996).
- [7] C. H. Bennett *et al.*, *Phys. Rev. Lett.* **76**, 722 (1996).
- [8] R. T. Thew and W. J. Munro, *Phys. Rev. A* **63**, R030302 (2001).
- [9] After [8], we use “concentration” to indicate an increase of both purity and entanglement.

- [10] J. G. Rarity and P. R. Tapster, *Phys. Rev. Lett.* **64**, 2495 (1990).
- [11] P. G. Kwiat *et al.*, *Phys. Rev. Lett.* **75**, 4337 (1995).
- [12] J. Brendel, N. Gisin, W. Tittel, and H. Zbinden, *Phys. Rev. Lett.* **82**, 2594 (1999).
- [13] C. A. Sackett *et al.*, *Nature* **404**, 256 (2000).
- [14] W. P. Bowen, R. Schnabel, P. K. Lam, and T. C. Ralph, *Phys. Rev. Lett.* **90**, 043601 (2003).
- [15] J. Bao, A. V. Bragas, J. K. Furdyna, and R. Merlin, *Nature Materials* **2**, 175 (2003).
- [16] A. G. White, D. F. V. James, P. H. Eberhard, and P. G. Kwiat, *Phys. Rev. Lett.* **83**, 3103 (1999).
- [17] A. G. White, D. F. V. James, W. J. Munro, and P. G. Kwiat, *Phys. Rev. A* **65**, 012301 (2001).
- [18] Y. S. Zhang, Y. F. Huang, C. F. Li, and G. C. Guo, *Phys. Rev. A* **66**, 062315 (2002).
- [19] W. J. Munro, D. F. V. James, A. G. White, and P. G. Kwiat, *Phys. Rev. A* **64**, R030302 (2001).
- [20] Note that for certain entanglement and mixedness parameterizations, the Werner states *are* the MEMS [21].
- [21] T. C. Wei *et al.*, *Phys. Rev. A* **67**, 022110 (2003).
- [22] P. Kwiat *et al.*, [quant-ph/0303040](https://arxiv.org/abs/quant-ph/0303040) (2003).
- [23] P. G. Kwiat, S. Barraza-Lopez, A. Stefanov, and N. Gisin, *Nature* **409**, 1014 (2001).
- [24] J. W. Pan, C. Simon, C. Brukner, and A. Zeilinger, *Nature* **410**, 1067 (2001); J. W. Pan *et al.*, *Nature* **423** 417 (2003); Z. Zhao *et al.*, *Phys. Rev. Lett.* **90** 207901 (2003).
- [25] T. Yamamoto, M. Koashi, S. K. Özdemir, and N. Imoto, *Nature* **421**, 343 (2003).
- [26] W. K. Wothers, *Phys. Rev. Lett.* **80**, 2245 (1998); V. Coffman and J. Kundu and W. K. Wothers, *Phys. Rev. A* **61**, 052306 (2000).
- [27] D. F. V. James, P. G. Kwiat, W. J. Munro, and A. G. White, *Phys. Rev. A* **64**, 052312 (2001).
- [28] The optical path length difference of the decoherers is not generally exactly  $140\lambda$ , causing an extra phase on the off diagonal elements. The phase is set to zero by slightly tipping one of the decoherers about its vertical axis.
- [29] A. J. Berglund, Dartmouth College B.A. Thesis, also [quant-ph/0010001](https://arxiv.org/abs/quant-ph/0010001) (2000); N. Peters *et al.*, *J. Quant. Inf. Comp.* **3**, 503 (2003).
- [30] As recently demonstrated [M. Barbieri, F. De Martini, G. Di Nepi, and P. Mataloni, [quant-ph/0303018](https://arxiv.org/abs/quant-ph/0303018) (2003); G. Di Nepi, F. De Martini, M. Barbieri, and P. Mataloni, [quant-ph/0307204](https://arxiv.org/abs/quant-ph/0307204) (2003)], one could instead use the spatial degree of freedom to induce decoherence; however, the states are then not suitable, e.g., for use in fiber optic systems, or where interference methods are needed.
- [31] R. Jozsa, *J. Mod. Optics* **41**, 2315 (1994).
- [32] The leading order normalized behaviors for the measures about a target value  $\rho_{MEMS_i}(r_0) \equiv \rho_i(r_0)$  by an amount  $\delta r \equiv r - r_0$  are  $S_L(\rho_i(r))/S_L(\rho_i(r_0)) \approx 1 - A_i \delta r$ ,  $T(\rho_i(r))/T(\rho_i(r_0)) \approx 1 + \frac{2}{r_0} \delta r$ , and  $F(\rho_i(r_0), \rho_i(r)) \approx 1 + B_i (\delta r)^2$ , where the subscript  $i$  denotes the class of MEMS, and the constants are given by  $A_I = \frac{2r_0 - 1}{r_0(1 - r_0)}$ ,  $A_{II} = \frac{2r_0}{\frac{4}{3} - r_0^2}$ ,  $B_I = \frac{-1}{4r_0(1 - r_0)}$ , and  $B_{II} = \frac{3}{2(9r_0^2 - 4)}$ .
- [33] In “twirling,” a random  $SU(2)$  rotation is independently performed on each photon pair.
- [34] Because it is presently very difficult to produce simultaneous indistinguishable *pairs* of photons, the filtration technique is *much* more efficient, e.g., where typically 20% of our incident ensemble of pairs survived, less than 0.005% would survive (estimated from the 2-fold and 4-

fold coincidence data reported in [24]) in the interference schemes, which require 4 photons.